AIP Journal of Applied Physics

Metal-oxide-semiconductor capacitors and Schottky diodes studied with scanning microwave microscopy at 18GHz

M. Kasper, G. Gramse, J. Hoffmann, C. Gaquiere, R. Feger, A. Stelzer, J. Smoliner, and F. Kienberger

Citation: Journal of Applied Physics **116**, 184301 (2014); doi: 10.1063/1.4897922
View online: http://dx.doi.org/10.1063/1.4897922
View Table of Contents: http://scitation.aip.org/content/aip/journal/jap/116/18?ver=pdfcov
Published by the AIP Publishing

Metal-oxide-semiconductor capacitors and Schottky diodes studied with scanning microwave microscopy at 18 GHz

M. Kasper,[1] G. Gramse,[2] J. Hoffmann,[3] C. Gaquiere,[4] R. Feger,[5] A. Stelzer,[5] J. Smoliner,[6] and F. Kienberger[7,a)]

[1]*Christian Doppler Laboratory for Nanoscale Methods in Biophysics, Johannes Kepler University of Linz, Gruberstrasse 40, 4020 Linz, Austria*
[2]*Biophysics Institute, Johannes Kepler University of Linz, Gruberstrasse 40, 4020 Linz, Austria*
[3]*METAS, National Metrology Institute of Switzerland, Lindenweg 50, 3003 Bern-Wabern, Switzerland*
[4]*MC2 technologies, 5 rue du Colibri, 59650 Villeneuve D'ascq, France*
[5]*Institute for Communications Engineering and RF-Systems, Johannes Kepler University, Altenberger Str. 69, 4040 Linz, Austria*
[6]*Vienna University of Technology, Institute for Solid State Electronics, Floragasse 7, 1040 Vienna, Austria*
[7]*Keysight Technologies Austria, Measurement Research Lab, Gruberstrasse 40, 4020 Linz, Austria*

(Received 28 July 2014; accepted 23 September 2014; published online 10 November 2014)

We measured the DC and RF impedance characteristics of micrometric metal-oxide-semiconductor (MOS) capacitors and Schottky diodes using scanning microwave microscopy (SMM). The SMM consisting of an atomic force microscopy (AFM) interfaced with a vector network analyser (VNA) was used to measure the reflection S11 coefficient of the metallic MOS and Schottky contact pads at 18 GHz as a function of the tip bias voltage. By controlling the SMM biasing conditions, the AFM tip was used to bias the Schottky contacts between reverse and forward mode. In reverse bias direction, the Schottky contacts showed mostly a change in the imaginary part of the admittance while in forward bias direction the change was mostly in the real part of the admittance. Reference MOS capacitors which are next to the Schottky diodes on the same sample were used to calibrate the SMM S11 data and convert it into capacitance values. Calibrated capacitance between 1–10 fF and $1/C^2$ spectroscopy curves were acquired on the different Schottky diodes as a function of the DC bias voltage following a linear behavior. Additionally, measurements were done directly with the AFM-tip in contact with the silicon substrate forming a nanoscale Schottky contact. Similar capacitance-voltage curves were obtained but with smaller values (30–300 aF) due to the corresponding smaller AFM-tip diameter. Calibrated capacitance images of both the MOS and Schottky contacts were acquired with nanoscale resolution at different tip-bias voltages. © *2014 AIP Publishing LLC*.
[http://dx.doi.org/10.1063/1.4897922]

INTRODUCTION

The development of novel nano-scale high speed materials and devices requires metrology tools capable of electrical characterization at the operating frequency and with nano-scale resolution. The non-destructive measurement of dopant profiles, carrier concentration, and device impedances including capacitance and conductivity are critical for newly emerging materials and devices such as carbon nanotubes, graphene, nanowires, spintronics, and varactors. A new scanning microwave microscope (SMM) has been developed to characterize the materials and devices at microwave frequencies with nanometer resolution.[1–4] The SMM has been shown to be capable of quantitative characterization of metals, semiconductors and dielectrics.[5] In addition quantitative nonlinear dielectric properties have been measured with SMM[4] and have been applied to the measurement of ferroelectric materials.[6] In SMM, a vector network analyzer (VNA) is interfaced with a standard atomic force microscope (AFM) to perform microwave network analysis at the nanoscale with frequencies ranging from 1 to 20 GHz.[7,8] The microwave signal generated by the VNA is transmitted via a coaxial cable to a conductive AFM tip. By comparing the incident RF signal to the back-reflected signal the S11 network parameters are extracted by the VNA. A standardized capacitance calibration sample of small capacitor plates is used to transfer the complex VNA amplitude and phase into absolute capacitance values ranging from roughly 0.1–10 fF (femto-Farad).[9] The capacitance calibration sample is a three-layer stacked sample of doped silicon, silicon oxide, and gold pads acting as small capacitors. With standard settings the SMM noise level is ~1 aF (atto-Farad).[9] The topographical image is acquired simultaneously to the complex S11 reflection parameters and a lateral resolution of 5–10 nm can be obtained with the SMM.

SMM covers a broad microwave frequency range of 1–20 GHz giving it an advantage over the scanning capacitance microscope (SCM) that operates at a single frequency below 1 GHz.[10] The broad frequency coverage and selectivity of SMM enables the study of materials properties including buried structural defects where the penetration depth is a function of frequency.[11] There are two measurement modes of SMM, and both modes can operate simultaneously, including the reflection mode for complex impedance imaging and the differential capacitance dC/dV mode for dopant profiling.[12] The combined impedance imaging and dC/dV imaging as well as

a)Author to whom correspondence should be addressed. Electronic mail: ferry_kienberger@keysight.com.

the broadband measurement capability offers several advantages of SMM compared to other methods like SCM[13,14] or scanning spreading resistance microscopy (SSRM).[15,16] SMM measurements at high frequencies around 20 GHz result in higher signal-to-noise ratio, because at a given capacitance (C) the circular frequency (ω) is directly related to the complex impedance change (Z), $Z = 1/j\omega C$.[17] Furthermore, while a high quality dielectric oxide layer is required for SCM measurements, SMM can be done also without an oxide layer as well as on non-conductive materials. Here, we develop a dedicated SMM measurement workflow for the measurement of metal-oxide-semiconductor (MOS) capacitors and metal-semiconductor Schottky diodes at GHz frequencies.

Schottky diodes are versatile circuit components used in several fields of electrical engineering including RF electronics and are available as discrete packaged components or as part of integrated circuits. For RF applications, the Schottky diodes are used for rectifying, detection and mixing of signals and in every case the nonlinear relationship between current and voltage is utilized.[18] The Schottky interface junction is formed between a metal (e.g., platinum) and a doped semiconductor (e.g., n-typed doped silicon). Compared to standard pn-diodes where the junction is formed between two different types of doped semiconductors, Schottky diodes have no significant minority charge carriers (e.g., holes for n-type Si) involved.[19] This is particularly advantageous when the diode is turned off. Before a standard pn-junction diode can turn off the free charge carriers of both polarities need to recombine which requires a significant reverse current peak flowing through the diode and also a certain amount of recovery time. For Schottky diodes, no recombination is required for turning them off making them ideal for fast high frequency electronics. An additional physical mechanism which affects the upper frequency limit of a diode is based on its series resistance and parallel capacitance. Both parasitic components act as a low-pass filter with a certain cutoff frequency.[18] While the resistance is mainly defined by the conductivity of the substrate the capacitance is formed by the semiconductor depletion zone and therefore depends on the thickness of the depletion zone and the electrode area. For a given current density, the Schottky diodes can employ a smaller electrode area resulting in higher cut-off frequencies in the range of few MHz up to 100 GHz and above.[18]

Full characterization of Schottky diodes includes the measurement of the I-V characteristic at DC as well as the measurement of network parameters in the desired GHz range. The latter is typically done using a wafer prober connected to a vector network analyzer as well as special test sets for connecting and contacting the Schottky diode.[20] Test sets include proper RF needles that contact specific test pads on the chip with a typical length scale in the range of 100 μm. The study of smaller device structures needs special contact test sets and for devices below 10 μm the wafer prober approaches its limitations. We show in this paper that for structures below 100 μm, the SMM can be efficiently used to study the electrical properties of Schottky diodes up to 20 GHz. In SMM, we use a standard conductive AFM tip representing a single ended contact with a referenced ground which is an alternative solution to the typical ground-signal-ground approach with wafer probers. We show also that the SMM tip can be used to establish and measure local nanoscale sized Schottky contacts on virtually any semiconductor substrate.

MATERIALS AND METHODS

SMM setup

A commercial transmission line SMM was used (Keysight Technologies, Chandler, USA) consisting of a

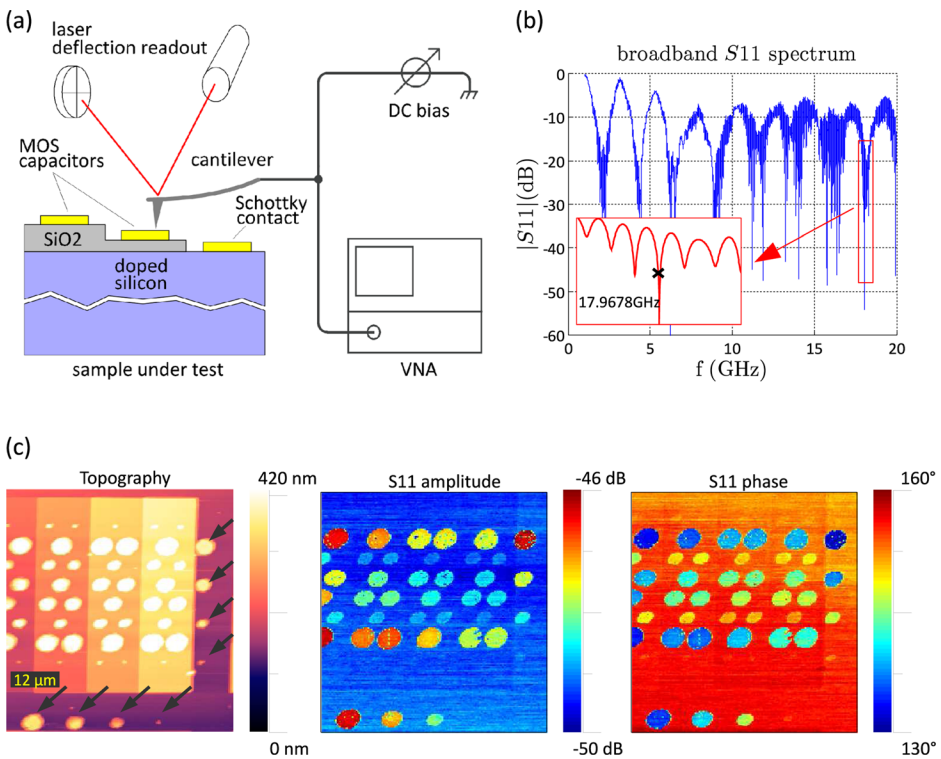

FIG. 1. Sketch of the SMM setup and images of the metal–oxide-semiconductor (MOS) and Schottky type electrical contacts. (a) The SMM combines an atomic force microscope (AFM) with a vector network analyser (VNA) using a transmission line and well controlled DC voltage bias conditions. (b) Broadband sweep of |S11| between 1 and 20 GHz shows main resonances every 2.2 GHz and additional high Q resonances created by the connection cable. Zoom in shows the chosen working frequency at 17.9678 GHz. (c) Topography and S11 images of the capacitance calibration sample with differently sized gold pads acquired with the SMM. The Schottky pads are labeled with arrows. The gold contact pads have different diameters (1 μm, 2 μm, 3 μm, and 4 μm) residing on SiO_2 layers of different thicknesses (50 nm, 100 nm, 150 nm, and 200 nm).

standard 5600 atomic force microscope (AFM) interfaced with a 20 GHz vector network analyzer (VNA) both from Keysight. AFM tips made from solid platinum (Rocky Mountain Nanotechnology, USA) were used. A sketch of the setup is shown in Figure 1. Inside the SMM nose cone a coaxial cable (50 Ω) forms a half wavelength resonator at 2.2 GHz that is terminated by a 50 Ω shunt.[7] The VNA sends a continuous microwave signal to the conducting AFM tip and detects the reflected microwave signal. This arrangement provides periodic notches with good sensitivity in the reflection coefficient S11 measured by the VNA (Figure 1(b)). The raw SMM data include the topographical image and the complex S11 reflection images. A closed loop scanner (scan size 100 x 100 μm^2) was used to have stable lateral x-y-position of the AFM tip on the gold pads.

Capacitance calibration sample

The capacitance calibration sample consists of several MOS contacts and Schottky contacts as shown in the topographical image acquired with the SMM (Figure 1(c)). The MOS contacts are gold pads residing on silicon oxide with different thicknesses and a doped silicon substrate (p-type) forming a back electrode, while the Schottky contacts are gold pads directly placed on the silicon substrate after pretreatment without an oxide in between. Platinum is used as intermediate layer to form a good quality Schottky contact. The diameters of the gold pad range from 1 to 4 μm and the thicknesses of the oxide ranges from 50 to 200 nm effectively forming parallel plate capacitors. The calibration samples were provided from MC^2 Technologies in France.

DC biasing

In order to generate well defined bias conditions for the Schottky contacts a DC source meter unit was used (SMU Keysight B2900; cf. Figure 2). The SMU offers both an accurate DC source as well as precise measurement channels for voltage and current. The resolution thereby is 100 nV and 100 fA, respectively. For the Schottky measurements, high currents are not involved therefore the four terminal Kelvin connection was not employed. The bias is applied via a 20 kΩ resistor to the cantilever. While the SMU also provides current limitation (set to 100 μA) the resistor approach was chosen to have additional separation between the biasing circuit and the RF circuit. Additionally, the resistor guarantees that no transient peak current occurs when for example the tip-sample contact is lost accidently. To prevent the DC bias voltage from being shorted by the RF ground connection the nose cone was equipped with a DC blocking capacitor (Figure 2).

Black box capacitance calibration workflow

The VNA acts as a reflectometer and measures the normalized reflection signal S11,m (scattering parameters) of the complete system (VNA calibration plane, Figure 2(a)). The amount of reflected signal directly at the tip S11,a depends on the tip-sample load impedance Z_{in} according to the following formula ($Z_{ref} = 50\ \Omega$ is the characteristic system impedance):

$$S_{11,a} = \frac{Z_{in} - Z_{ref}}{Z_{in} + Z_{ref}}.$$

To calibrate the electric response of the SMM and to transfer the S11 values into calibrated capacitance values we apply a black box calibration algorithm.[17,21] The black box contains all circuit elements between the tip and the calibration plane of the VNA such as C_{stray}, C_{return}, the shunt resistor and all cables. To determine the black box three individual known MOS standards which are sufficiently different in their electrical behavior are measured and the results are used to compute three complex correction coefficients e_{00}, e_{01}, and e_{11}, according to the following formula:

$$S_{11,m} = e_{00} + e_{01}\frac{S_{11,a}}{1 - e_{11}S_{11,a}}.$$

The resulting transfer function is then used to convert the S11 data into calibrated capacitance values[17] and the

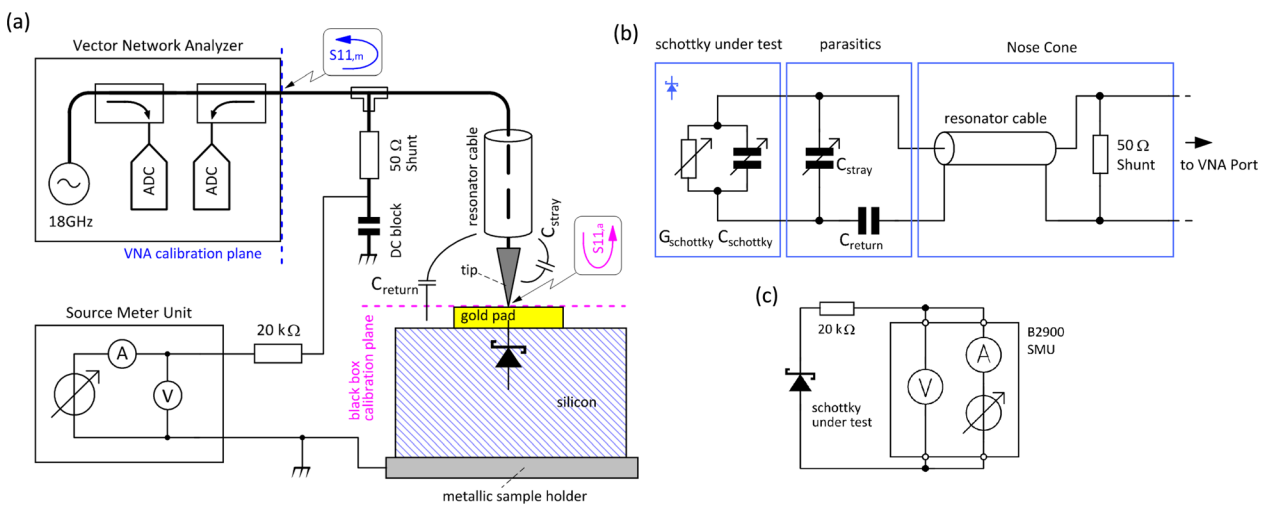

FIG. 2. Experimental SMM setup and equivalent circuitry for the Schottky contact. (a) The reflection coefficient S11,m of the AFM tip connected to the coaxial resonator cable which depends on the tip-sample impedance is measured by the VNA. The bias voltage is generated by a Source Meter Unit (SMU). (b) Equivalent RF circuit. (c) Equivalent DC bias circuit.

calibration plane is effectively moved directly to the tip (black box calibration plane, Figure 2(a)). To calculate the capacitance of the reference MOS standards a series model consisting of an oxide capacitance C_{ox} and a depletion capacitance C_{depl} is used. Both capacitances are evaluated by use of the parallel plate capacitor formula $C = \varepsilon_0\varepsilon_r A/d$ with ε_0 the vacuum permittivity, ε_r the relative dielectric constant of the corresponding material (SiO_2 and Si), A the gold pad area, and d the thickness of the corresponding layer (d_{ox} and d_{depl}). The oxide thickness d_{ox} is given by the sample specification and the depletion zone thickness d_{depl} is calculated according to the formula:

$$d_{depl} = \mathrm{sqrt}(k^*T^*e_{,Si}/(N_a{}^*q^2)),$$

with k the Boltzmann constant, T the absolute temperature (298 K), $\varepsilon_{,Si}$ the permittivity of silicon, N_a the number of acceptors due to doping (10^{17}/cm^3 for the used sample) and q the elementary charge.[17,21]

RESULTS AND DISCUSSION

The AFM tip was positioned onto the various gold pads of the MOS capacitors and Schottky contacts by acquiring a topographical image (Figure 1) and moving the tip to the corresponding positions using a closed loop scanner. The Schottky gold contacts are placed directly on the silicon substrate without an intermediate SiO_2 layer. DC measurements were done with the source-meter unit (SMU), while RF measurements were done at 18 GHz with the SMM (Figure 2). The Schottky contact is modelled as a variable capacitance in parallel with a variable conductivity (Figure 2(b)). Both elements are changing with the bias voltage. In parallel, there is also a stray capacitance (C_{stray}) formed by the AFM cantilever which slightly changes when the tip is moved laterally to different positions. The RF return path between sample and AFM tip holder is formed by capacitive coupling which is represented by a series capacitance (C_{return}). The influence of both the stray and the return capacitance is corrected in the calibration algorithm (cf. Materials and Methods). The quality and stability of the contact between AFM tip and gold pad are important for electrical measurements and is influenced by many factors including contact force, tip geometry, dirt, and water films adsorbed on the sample surface. Therefore, the forward current of the Schottky contacts was measured with the SMU and used as quality criteria of the tip-sample contact.

Figure 3 shows the raw reflection coefficient S11 of four MOS capacitors and four Schottky contacts acquired with the SMM at 18 GHz. The measurement series on a single gold pad consists of a voltage bias sweep between −6 V (forward mode on the p-type silicon substrate) and +6 V (reverse mode). At each bias point, the reflection coefficient, voltage and current values are measured 25 times allowing for data averaging. The SMM frequency is held constant during the whole measurement. While the broadband characteristic of the SMM allows to measure also at lower frequencies starting at 1 GHz, the 18 GHz were used because of increased sensitivity at higher frequencies.[7,17] To optimize the signal-to-noise

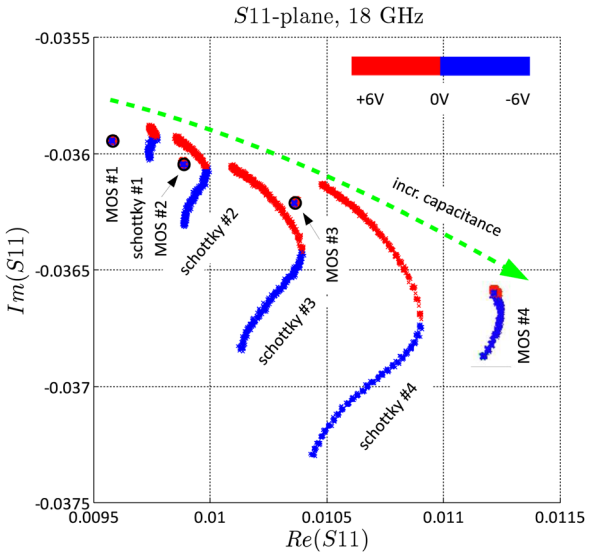

FIG. 3. SMM reflection coefficient S11 measurements at 18 GHz shown in the complex plane. The S11-voltage trajectories of four MOS reference capacitors and four Schottky contacts are shown. The bias voltage is swept from +6 V to −6 V. The Schottky contacts (#1 1 μm diameter; #2 2 μm diameter; #3 3 μm diameter; #4 4 μm diameter) show a specific 90° change in their trajectories at zero bias voltage when the impedance changes from dominant capacitive to dominant resistive. The MOS contacts #1 (200 nm oxide), #2 (150 nm oxide), and #3 (100 nm oxide) stay constant during the bias sweep and only #4 (50 nm oxide) shows some deviation from ideal behavior at larger negative biases. For the capacitance calibration procedure only the zero bias capacitance of the MOS contacts are used (marked with circles).

(SNR) ratio of the system, the measurement frequency was tuned to the exact value of 17.9678 GHz (Figure 1(b)). Good working points in terms of SNR are at frequencies which provide high-Q notches in the S11 magnitude versus frequency plot with typical S11 values around −30 dB. The complex S11 plane in Figure 3 shows the measured spectroscopy curves of the various gold pads which are in close proximity to the origin (Im(S11) = Re(S11) = 0) due to the small magnitude of the reflection coefficient of −30 dB. Because the reflection coefficient is a relative quantity, both the real and the imaginary axes are dimensionless and the maximum possible value in a passive microwave system is 1.

In Figure 3, the MOS capacitors are formed by the gold pad on silicon oxide and a doped silicon substrate and can be described by the simple parallel plate capacitance $C = \varepsilon_0\varepsilon_r A/d$. The depletion zone in the doped silicon substrate is responsible for a small variation in capacitance with varying DC bias voltage. However, because of the serial circuit of oxide capacitance C_{ox} and depletion zone capacitance C_{depl}, the small thickness of the depletion zone and the corresponding large capacitance results only in a small influence on the overall MOS capacitance. Typical values for the 1 μm diameter gold pad on a 200 nm oxide are $C_{depl} \sim 14$fF and $C_{ox} \sim 0.14$ fF. No significant change of the MOS capacitance with the DC bias is therefore expected. While the MOS capacitors on the thick oxides (#1 to #3; 100 nm to 200 nm) show this ideal behavior, only the MOS capacitor on the thin oxide (#4; 50 nm) shows some impedance changes at high negative bias voltages.

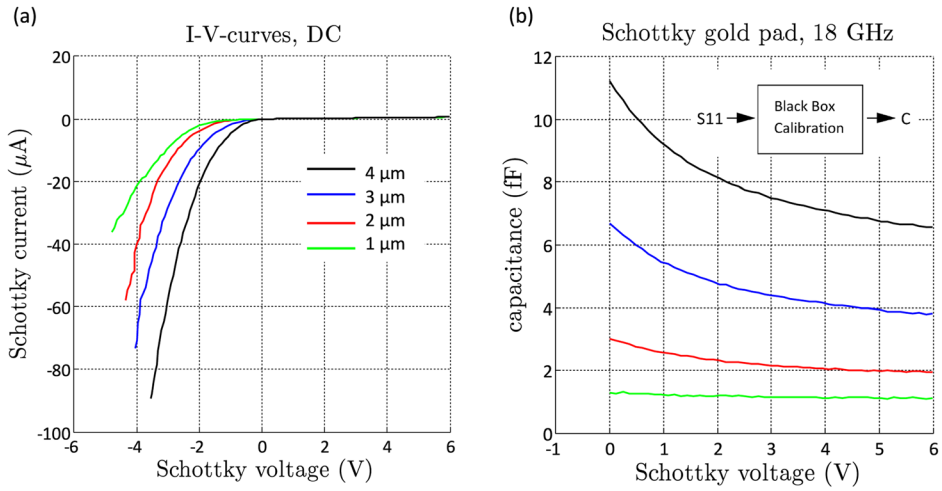

FIG. 4. DC and RF measurements of the Schottky contacts. (a) I-V curves of the four different Schottky contacts. The DC voltage and current measurements were done with the AFM tip in contact with the Schottky gold pads. The current is measured directly with the SMU and the voltage is corrected for the voltage drop at the 20 kΩ resistor. (b) RF measurements of the Schottky contacts. Calibrated Schottky capacitance curves were derived from SMM S11 measurements at 18 GHz after applying the standard black-box calibration algorithm.[21] The C-V curves show parabolic behavior in line with the modeling results.

For the Schottky contacts in Figure 3, the bias is swept also between +6 V (red) and −6 V (blue) with the zero bias being the position where the color changes. In the reverse biased region (positive voltage values in red) the Schottky depletion zone thickness is controlled by the bias voltage and therefore the capacitance is changed. Higher voltages increase the depletion zone thickness and the capacitance has the smallest value at the highest positive bias. This is in line with the green curve showing the capacitance direction in the complex S11 plane. As the bias voltage becomes smaller and eventually goes through zero the capacitance increases to a maximum value, and the curves follow a 90° change in the complex plane. At a slightly negative bias voltage (about −1 V; blue curve) the Schottky contacts start to conduct, and the forward current increases as well as the real part of the Schottky admittance (i.e., the conductivity) starts to increase. As the bias voltage is decreased further the real part becomes more dominant (blue curve) and finally at high forward currents (∼50 μA) the Schottky impedance has changed to an almost completely conductive type of behavior. In the complex plane, this results in a characteristic knee (90° change) of the reflection coefficient trajectory at zero bias voltage. The transfer function of the SMM can be treated as conformal transformation which is angle conserving, therefore the 90° angle between the real and imaginary part of the impedance follows also this ideal behavior in the reflection coefficient plane.[18,22]

Figure 4 shows the DC current and RF capacitance of the four Schottky contacts. DC measurements have been performed with the SMU and Figure 4(a) presents the typical Schottky diode I-V characteristics.[19] As the substrate is a p-type doped silicon wafer the turn on voltage is at negative values around −0.7 V. The diode behavior is observed for all Schottky contacts with a significant resistance contribution that can be adjusted with the bias condition. The RF Schottky capacitance in Figure 4(b) was derived by calibrating the SMM S11 data using the black box algorithm.[21] Three MOS capacitors were used as reference and the three complex calibration parameters were determined to transfer the reflection S11 measurements into calibrated capacitance values. The RF C-V curves for the Schottky contacts show the typical behavior with high capacitance at small voltages.[19] Also the capacitance scales properly with the gold pad area with the largest gold pad showing ∼11 fF at zero bias voltage while the smallest gold pad shows only ∼1 fF. The Schottky C-V curve is significantly different to the sigmoidal C-V curves acquired

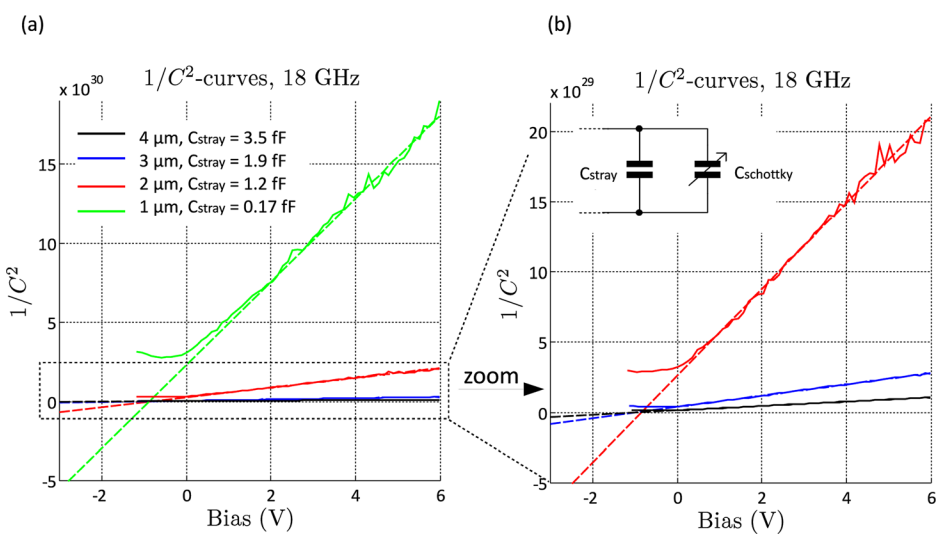

FIG. 5. $1/C^2$ versus the bias voltage plotted for the four gold pad Schottky contacts after subtracting the constant parasitic (C_{stray}) capacitance automatically by an iterative algorithm. A zoom into the three smallest Schottky contacts is given in (b). A linear $1/C^2$ behavior is expected for the ideal Schottky capacitance ($C_{schottky}$). The intersection with the voltage axis indicates the barrier height of the Schottky contact.

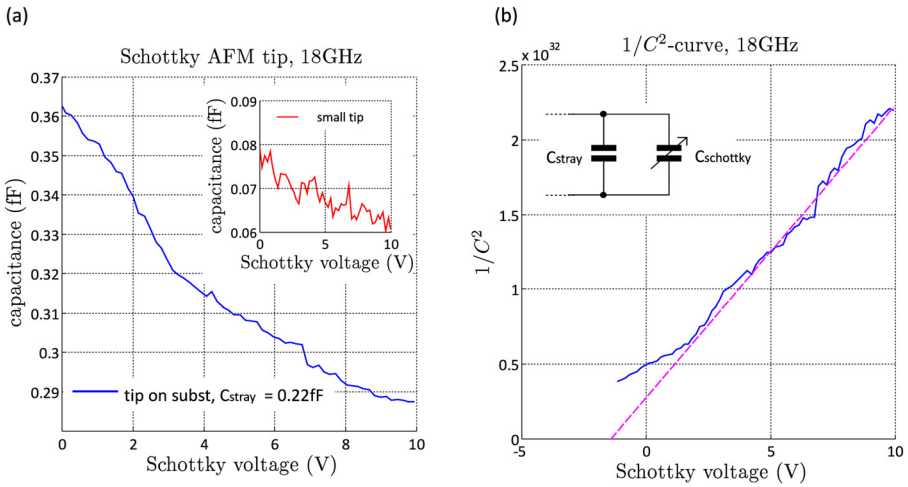

FIG. 6. Capacitance measurements of Schottky contacts formed directly by the AFM tip on the substrate without gold pads. The capacitance of the AFM tip is plotted versus the tip-bias voltage (a). The measurement was done at 18 GHz and the bias was swept between 10 and +10 V. 100 curves were acquired and the average data is shown (blue trace). The inset shows the measurement with a smaller tip. $1/C^2$ versus bias voltage curves are shown in (b) with the parallel stray capacitance removed.

on the MOS capacitors (data not shown; cf. Ref. 12) and both Schottky and MOS spectroscopy curves follow the ideal behavior uunder the assumption of a constant dopant concentration along the depletion cone.[19]

Figure 5 shows the capacitance $1/C^2$ versus the bias voltage plotted for the four Schottky contacts after subtracting the constant parasitic (C_{stray}) capacitance. The parasitic capacitance was removed by an automated iterative algorithm that starts at zero subtraction capacitance and successively adapts it until the quadratic error between the data and a quadratic function is minimized. For an ideal Schottky contact $1/C^2$ is expected to be linear in accordance to the experimental results.[19]

After measuring the Schottky behavior on the micrometer sized gold pads the same workflow was applied without the gold pads by using the metallic nanometer sized AFM tip as Schottky contact (Figure 6). Figure 6(a) shows the calibrated capacitance versus bias voltage plotted for the platinum AFM tip in contact with the p-type silicon substrate. Similar like done on the gold pads, the reflection coefficients were measured at 18 GHz while sweeping the bias voltage from −6 to +10 V. The black box calibration was applied to transfer S11 into capacitance data. Compared to the measurements on the gold pads here the contact force was slightly increased to get proper electrical contact on the native oxide layered silicon. The absolute capacitance values are smaller (∼300 aF in Figure 6(a)) compared to the gold pad measurements (e.g., 3 fF at 2 μm diameter) because the electrode is defined by the AFM tip diameter which is typically smaller than a micrometer. Experiments done with smaller tip diameters result in smaller capacitance values (e.g., 70 aF in Figure 6(a), inset). Due to the smaller electrode size and capacitance values an average of 100 curves was taken with each individual C-V measurement taking ∼1 s. Similar to the Schottky gold pad measurements, the AFM-tip capacitance follows the linear $1/C^2$ behavior (Figure 6(b)). The AFM-tip diameter can be estimated by comparison with the Schottky gold pad measurements according to $d^4/C(V)^2 = \text{constant}$, with d the electrode diameter and C(V) the capacitance at a given voltage V.[19] Under the assumption of equal barrier voltages, the AFM tip diameter can be estimated to 0.5 μm for 300 aF and 0.2 μm for 70 aF tip capacitance. While the diameters are in line with scanning electron microscopy images of the AFM tips (not shown) a pretreatment was done for the Schottky contacts to guarantee the quality and uniformity which is not the case for the AFM-tip measurements.

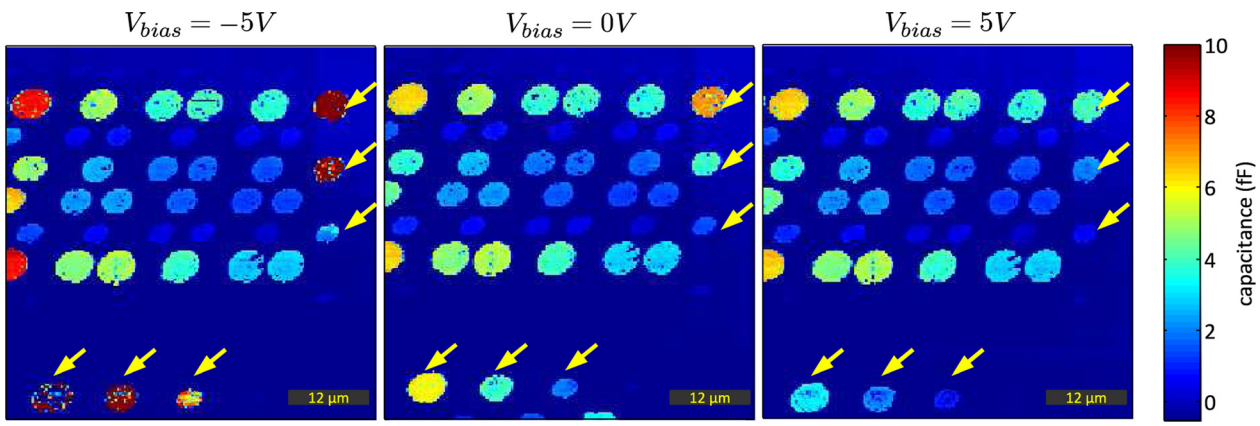

FIG. 7. SMM capacitance images of the MOS and Schottky contacts at different tip-bias voltages. The VNA amplitude and phase images were acquired at different DC tip-bias voltages and transferred into calibrated capacitance using the blackbox calibration algorithm. The Schottky diodes change their capacitance significantly (cf. arrows).

Figure 7 shows SMM capacitance images of both the MOS and Schottky contacts at different tip-bias conditions. While all the above-mentioned experiments were done with the AFM-tip at a fixed lateral position here we did standard SMM scanning resulting in topography, PNA amplitude and phase images (cf. Figure 1(c)). Three MOS contact pads were used for the black-box calibration and calibrated capacitance images were plotted at −5 V, 0 V, and +5 V tip bias. The Schottky contacts show a significant change in the capacitance, while most of the MOS contact stays constant with respect to the tip-bias voltage. Only the MOS contacts at the thin oxide layer show some capacitance change at larger negative tip bias voltages similar as obtained in Figure 3.

CONCLUSION

In SMM, the AFM tip is used as a nanoscale imaging probe enabling correlated topography and microwave characterization of MOS capacitors and Schottky diodes formed by micrometer sized gold contact pads. The SMM measurements allowed characterizing the electrical behavior of the metallic contacts with respect to the voltage bias condition and the geometrical size of the gold pads. The variations of the SMM S11 reflection coefficients at 18 GHz were directly related to the equivalent electrical model of the Schottky diodes. By changing the bias conditions, the surface depletion charge between the gold pad contact and the silicon substrate was adjusted and the equivalent complex admittance $Y = G + jB$ of the Schottky diode was measured with the SMM. Typical values for the susceptance B range from 10 μS to 1 mS corresponding to 0.1–10 fF at 18 GHz with an accuracy of the capacitance values of 10–20%.[9,21] Capacitance images were acquired showing both the MOS and Schottky contacts at different tip-bias voltages. As the silicon substrate is p-type doped the reverse bias region is at positive voltages, while the forward region is at negative voltages. The measured reflection coefficient trajectories have a 90° knee when the bias condition goes through zero and the impedance characteristic changes from dominant capacitive in reverse mode to dominant conductive in forward mode. In reverse mode, the DC-currents are very small resulting in a low parallel conductance (below 0.1 μS) or equivalent high insulating serial resistance (several tens of MΩ), while the capacitance can be adjusted by varying the bias voltage. After the bias voltage changes the sign and the turn on voltage is reached current starts to flow and increases rapidly with bias voltage due to the exponential diode characteristic. In this region, a small change in bias voltage causes a large variation in conductance. Also the capacitance increases further in forward mode but is effectively shorted by the conductance at significant forward bias. The diode behavior and the variable conductance in forward mode were observed for all Schottky contacts. Accordingly, the Schottky contacts can be potentially used in future studies as adjustable resistance calibration spots for complex impedance SMM measurements. Similarly, the differently sized MOS gold pads are used in the black-box algorithm to calibrate the SMM capacitance. The measurement workflow was developed on the micrometer sized gold pad contacts and finally also tested with the AFM tip itself forming the Schottky diode. This shows an interesting application of the SMM for direct characterization of semiconductor surfaces under bias control. In summary we have shown how the SMM can be used to study different electric MOS and Schottky contacts up to 20 GHz by developing proper measurement and analysis workflows.

ACKNOWLEDGMENTS

The authors would like to thank O. Lang, A. Hornung, and P. Hinterdorfer from JKU (Austria), and C. Rankl, M. Moertelmaier, E. Brinciotti, M. Richter, and H. Tanbakuchi from Agilent Technologies for helpful technical discussions. This work has been supported by the EU FP7 (NMP2011280516, VSMMARTNano) and the Austrian Christian Doppler Society.

[1]H. Tanbakuchi *et al.*, "Nanoscale materials and device characterization via a scanning microwave microscope," in *IEEE International Conference on Microwaves, Communications, Antennas and Electronics Systems - COMCAS*, pp. 574–577 (2009).
[2]B. Rosner and D. W. van der Weide, "High-frequency near-field microscopy," Rev. Sci. Instrum. **73**(7), 2505–2526 (2002).
[3]S. M. Anlage, V. V. Talanov, and A. R. Schwartz, *Principles of Near-Field Microwave Microscopy*, in *Scanning Probe Microscopy: Electrical and Electromechanical Phenomena at the Nanoscale*, edited by S. V. Kalinin and A. Gruverman (Springer-Verlag, New York, 2007), Vol. 1, pp. 215–253.
[4]D. E. Steinhauer *et al.*, "Quantitative imaging of dielectric permittivity and tunability with a near-field scanning microwave microscope," Rev. Sci. Instrum. **71**, 2751–2758 (2000).
[5]A. Imtiaz, T. M. Wallis, and P. Kabos, "Near-field scanning microwave microscopy: An emerging research tool for nanoscale metrology," IEEE Microwave Mag. **15**(1), 52–64 (2014).
[6]D. E. Steinhauer and S. M. Anlage, "Microwave frequency ferroelectric domain imaging of deuterated triglycine sulfate crystals," J. Appl. Phys. **89**, 2314–2321 (2001).
[7]H. Tanbakuchi *et al.*, "Semiconductor material and device characterization via scanning microwave microscopy," In *Compound Semiconductor Integrated Circuit Symposium (CSICS)* (IEEE, 2013), pp. 1–4.
[8]T. Kazuhisa, A. Makoto, and M. Teuaki, "Sensitivity analysis of scanning microwave microscopy for nano-scale dopant measurements in Si," J. Appl. Phys. **112**(10), 104325–4 (2012).
[9]H. P. Huber *et al.*, "Calibrated nanoscale capacitance measurements using a scanning microwave microscope," Rev. Sci. Instrum. **81**(11), 113701–113710 (2010).
[10]J. Smoliner *et al.*, "Scanning microwave microscopy/spectroscopy on metal-oxide-semiconductor systems," J. Appl. Phy. **108**(6), 64315–64317 (2010).
[11]C. Plassard *et al.*, "Detection of defects buried in metallic samples by scanning microwave microscopy," Phys. Rev. B **83**(12), 121409 (2011).
[12]H. P. Huber *et al.*, "Calibrated nanoscale dopant profiling using a scanning microwave microscope," J. Appl. Phys. **111**(1), 014301–10 (2012).
[13]P. J. Hansen *et al.*, "Scanning capacitance microscopy imaging of threading dislocations in GaN films grown on (0001) sapphire by metalorganic chemical vapor deposition," Appl. Phys. Lett. **72**(18), 2247–2249 (1998).
[14]J. R. Matey and J. Blanc, "Scanning capacitance microscopy," J. Appl. Phys. **57**(5), 1437–1444 (1985).
[15]P. De Wolf *et al.*, "Two-dimensional carrier profiling of InP structures using scanning spreading resistance microscopy," Appl. Phys. Lett. **73**(15), 2155–2157 (1998).
[16]P. Eyben *et al.*, "Scanning spreading resistance microscopy and spectroscopy for routine and quantitative two-dimensional carrier profiling," J. Vacuum Sci. Technol. B **20**(1), 471–478 (2002).
[17]G. Gramse *et al.*, "Calibrated complex impedance and permittivity measurements with scanning microwave microscopy," Nanotechnology **25**(14), 145703 (2014).
[18]D. M. Pozar, *Microwave Engineering*, 4th ed. (John Wiley & Sons, 2011).

[19]S. M. Sze and K. K. Ng, *Physics of Semiconductor Devices*, 3rd ed. (John Wiley & Sons, New York).
[20]Cascade Microtech Inc., *On Wafer Vector Network Analyzer Calibration & Measurements* (2002).
[21]J. Hoffmann *et al*., "A calibration algorithm for nearfield scanning microwave microscopes," in *12th IEEE Conference on Nanotechnology* (2012), pp. 1–4.
[22]B. C. Wadell, *Transmission Line Design Handbook* (Artech House, 1991).